

RADAR OBSERVATIONS OF E-CLASS ASTEROIDS 44 NYSA AND 434 HUNGARIA

Michael K. Shepard, Bloomsburg University, Bloomsburg, PA 17815

Karelyn M. Kressler, Earlham College, Richmond, IN 47374

Beth Ellen Clark, Ithaca College, Ithaca, NY 14853

Maureen E. Ockert-Bell Ithaca College, Ithaca, NY 14853

Michael C. Nolan, NAIC/Arecibo Observatory, HC 3 Box 53995, Arecibo, PR 00612

Ellen S. Howell, NAIC/Arecibo Observatory, HC 3 Box 53995, Arecibo, PR 00612

Christopher Magri, University of Maine at Farmington, Farmington, ME 04938

Jon D. Giorgini, Jet Propulsion Laboratory, Pasadena, CA 91109

Lance A.M. Benner, Jet Propulsion Laboratory, Pasadena, CA 91109

Steven J. Ostro, Jet Propulsion Laboratory, Pasadena, CA 91109

Manuscript pages: 11

Figures: 2

Tables: 4

Submitted to Icarus Sept 6, 2007

Revised Dec 5, 2007

Running Head: Radar Observations 44 Nysa and 434 Hungaria

Corresponding author:

Michael K. Shepard
Dept. of Geography and Geosciences
Bloomsburg University of Pennsylvania
400 E. Second St.
Bloomsburg, PA 17815
570-389-4568 (ph.)
570-389-3028 (fax)
mshepard@bloomu.edu

Keywords: ASTEROIDS; ASTEROIDS, COMPOSITION; SURFACES, ASTEROIDS; RADAR

Abstract

We observed the E-class main-belt asteroids (MBAs) 44 Nysa and 434 Hungaria with Arecibo Observatory's S-band (12.6 cm) radar. Both asteroids exhibit polarization ratios higher than those measured for any other MBA: Nysa, $\mu_c = 0.50 \pm 0.02$ and Hungaria, $\mu_c = 0.8 \pm 0.1$. This is consistent with the high polarization ratios measured for every E-class near-Earth asteroid (NEA) observed by Benner et al. (submitted to Science, 2007) and suggests a common cause. Our estimates of radar albedo are 0.19 ± 0.06 for Nysa and 0.22 ± 0.06 for Hungaria. These values are higher than those of most MBAs and, when combined with their high polarization ratios, suggest that the surface bulk density of both asteroids is high. We model Nysa as an ellipsoid of dimension 113 x 67 x 65 km ($\pm 15\%$) giving an effective diameter $D_{\text{eff}} = 79 \pm 10$ km, consistent with previous estimates. The echo waveforms are not consistent with a contact binary as suggested by Kaasalainen et al (A&A 383, L19-L22, 2002). We place a constraint on Hungaria's maximum diameter, $D_{\text{max}} \geq 11$ km consistent with previous size estimates.

INTRODUCTION

The E-class asteroids are defined (Zellner et al. 1977; Tholen, 1984; Tholen and Barucci, 1989) as those having flat to red, featureless spectra like their spectrally degenerate cousins, the P and M asteroids, but differentiated from them by high visual albedos, taken somewhat arbitrarily to be $p_v > 0.3$. They are usually interpreted to be composed of iron-free silicate minerals such as enstatite and are believed to be analogous to enstatite achondrites (aubrites) (Bell et al. 1989).

Only five E-class asteroids, all near-Earth (NEAs), have been previously observed by radar (Benner et al. 2007). The most unusual feature of these observations is that all exhibit very high polarization ratios, $\mu_c \geq 0.8$, defined as:

$$\mu_c = \frac{\sigma_{SC}}{\sigma_{OC}} \quad (1)$$

where σ_{SC} is the radar cross-section (cross-section, in km^2 , of a metal sphere at the same distance with the same echo power) in the same circular (or unexpected) sense and σ_{OC} is that in the opposite circular (or expected) sense. Values larger than zero are caused by wavelength-scale near-surface roughness and inhomogeneities and/or subsurface or multiple scattering. Smooth surfaces have polarization ratios approaching 0.0, while some extremely rough or volumetrically complex surfaces have values equal to or even exceeding unity (Campbell and Campbell, 1992; Ostro et al. 2002; Campbell and Campbell, 2006; Harmon and Nolan, 2007; Benner et al. 2007). Polarization ratios for the common S and C-class NEAs have a mean of 0.28 ± 0.10 (Benner et al. 2007) while main-belt asteroids (MBAs) exhibit a significantly lower mean of 0.14 ± 0.10 (Magri et al. 2007a). This difference is thought to be due to the larger size and older surface age of MBAs relative to NEAs. A thicker and older regolith would be expected to have a lower density of wavelength-scale scatterers. Because all the E-class NEAs observed by radar exhibit high polarization ratios, Benner et al. (2007) suggest a composition-related cause. Hypotheses include the presence (at or near the surface) of wavelength-scale crystals of enstatite which are commonly observed in aubrites, highly brecciated surfaces, or some unique collisional history related to their formation.

We observed the main-belt E-class asteroids 44 Nysa and 434 Hungaria in 2006 with the S-band (12.6 cm) radar at Arecibo observatory. Observation and reduction techniques were the same as described in our previous papers (see Magri et al. 2007a). Table 1 lists the known physical properties of these objects.

RESULTS

44 Nysa

IRAS observations lead to estimates of Nysa's effective diameter (diameter of a sphere with a volume equal to that of the asteroid) $D_{\text{eff}} = 71 \pm 5$ km and optical albedo $p_v = 0.55 \pm 0.07$ (Tedesco et al. 2002). Based on an analysis of dozens of lightcurves, Taylor and Tedesco (1983) report a pole position of $(\lambda, \beta) = (100^\circ, +60^\circ) \pm 10^\circ$ and a sidereal rotation period $P = 6.421417 \pm 0.000002$ h. Kaasalainen et al. (2002) use 63 lightcurves to generate a cone-shaped convex model ($a/b \sim 1.6$, $a/c \sim 1.9$) for Nysa and report an identical period $P = 6.421417 \pm 0.000001$ h and a consistent pole $(\lambda, \beta) = (98^\circ \pm 2^\circ, +58^\circ \pm 3^\circ)$ and further suggest that Nysa might be a contact binary. Tanga et al. (2003) used the Hubble Space Telescope Fine Guidance Sensors (HST/FGS) to derive Nysa's angular diameter and shape. They assumed a pole position $(102^\circ, +50^\circ)$ and modeled Nysa as a triaxial ellipsoid of dimensions $119 \times 69 \times 69$ km ($D_{\text{eff}} = 83$ km, $a/b \sim 1.6$, $a/c \sim 1.6$), somewhat larger than the IRAS value. Their constraint on the a/c axis ratio was considered good, but their constraint on the a/b axis ratio was considered poor. They looked for evidence of bifurcation and could neither confirm nor rule it out.

We observed 44 Nysa on three nights, 22-24 Dec 2006 (Table 2). We obtained 7 continuous wave (CW) runs with a total OC SNR of 52 (Figure 1). Radar parameters for individual runs and the total experiment are listed in Table 3. Nysa is notable for its high polarization ratio $\mu_c = 0.50 \pm 0.02$, the second highest measured for a MBA and significantly higher than the majority of NEAs (Benner et al. 2007).

Our rotational coverage included all sides and had sufficient SNR to estimate an ellipsoidal shape model for Nysa using methods described by Magri et al. (2007b). The primary purpose of this modeling was to see which size estimate (IRAS ~ 71 km or Tanga et al. ~ 83 km) was more consistent with our data. We assumed the Kaasalainen et al. (2002) period and pole, giving a sub-radar latitude of 28° , and began with a base ellipsoid model similar to their shape,

110 x 68 x 57 km ($a/b \sim 1.6$, $a/c \sim 1.9$, $D_{\text{eff}} = 75$ km). We tested additional ellipsoid models of greater and lesser size and different axis ratios. Because Nysa has such a high polarization ratio, we summed both senses of polarization within each run forming a series of total power spectra, and smoothed these to an effective frequency of 20 Hz ($\sim 5\%$ of the total bandwidth) to increase the total SNR for shape modeling. Adding the SC component to our signal increases our ability to detect the spectral edges. We assumed a cosine scattering law of the form

$$\frac{d\sigma}{dA} = R(C + 1) \cos^{2C} \theta$$

where σ is the total radar cross-section, A is a target surface area, R is the Fresnel reflectivity at normal incidence, θ is the scattering angle, and C is a roughness parameter related to the root mean square (RMS) slope angle (Mitchell et al. 1996). Larger values of C indicate more specular scattering. We fixed C at 0.5 (essentially making this a diffuse scattering law) to account for the additional diffuse component of our summed signal. We had good leverage on the a/b axis ratio but less on the a/c axis ratio because Nysa did not move significantly during our observation window. As noted earlier, Tanga et al. (2002) constrain $a/c \sim 1.6$ using the HST/FGS. Our best fit ellipsoids have an a -axis of 113 ± 10 km with an a/b axis ratio of 1.7 ± 0.1 (b -axis of 67 ± 10 km) and an a/c axis ratio of 1.6-1.9 (c -axis of 65 ± 12 km) giving $D_{\text{eff}} = 79 \pm 10$ km, more consistent with the Tanga et al size estimate, but within the uncertainties of the IRAS value. Our diameter estimate leads to a visual albedo of $p_v = 0.44 \pm 0.10$ and radar albedo of $\hat{\sigma}_{oc} = 0.19 \pm 0.06$.

Our observations cover an entire rotation but have gaps of up to 90° in rotation phase. With that caveat, inspection of the CW spectra in Figure 1 shows no strong evidence for bifurcation. A number of bifurcated asteroids have been observed by radar, and the spectral waveform of such a target is typically bimodal. The central dip in the OC spectrum of run #4 suggests that Nysa has a significant concavity, but the dip is not pronounced enough to indicate bifurcation. The SC spectrum of this run does show bimodal behavior, but this suggests that the area around the sub-radar longitude is much smoother than the surrounding edges. It may be that Nysa is a contact binary, but in this data set it does not appear to be cleanly split into two well separated masses.

434 Hungaria

434 Hungaria has an estimated diameter of $D_{\text{eff}} = 11 \pm 2$ km, optical albedo $p_v = 0.4 \pm 0.07$ (Morrison, 1977), and long rotation period $P = 26.5$ h (Harris and Young, 1983; Harris et al. 1999; Durech, personal comm.). Kelley and Gaffey (2002) recently examined high resolution visible/near-infrared spectra and found spectral evidence for one or more mineral phases other than enstatite but were unable to definitively identify them.

We observed Hungaria on four nights, 14,16,18,20 May 2006 (Table 2). Our runs were taken on alternating nights because of the nearly synchronous relationship between Hungaria and Earth's rotation periods. We obtained 22 continuous wave (CW) runs with a total OC SNR of 15 (Figure 2). Because of Hungaria's slow rotation period and the relatively low SNR of individual runs, we summed each day's runs for our analysis; this results in a rotational smear of $\sim 35^\circ$ for each day's sum and gives coarse rotational coverage. Radar parameters for daily sums and the total experiment are listed in Table 4. Hungaria is notable for its high polarization ratio $\mu_c = 0.8 \pm 0.1$, surpassing Nysa as the highest for an MBA.

To better estimate Hungaria's radar bandwidth, we folded our spectra about 0 Hz to increase SNR, then summed the OC and SC components (Fig. 2) giving a total SNR of 24. Our best bandwidth estimate is $12 +3/-1$ Hz, leading to $D_{\text{max}} \geq 11$ km. Using sparse photometric methods (Durech et al. 2007), Durech (personal comm.) estimates Hungaria's pole to be (λ, β) $(119^\circ, +67^\circ) \pm 20^\circ$, leading to a subradar latitude of $27^\circ \pm 20^\circ$ and $D_{\text{max}} = 13 +4/-2$ km. This is consistent with the Morrison (1977) diameter estimate. We measured an OC cross section of $\sigma_{\text{OC}} = 21 \pm 6$ km² giving a radar albedo $\hat{\sigma}_{\text{OC}} = 0.22 \pm 0.06$.

Discussion

The most surprising result of these observations is the high polarization ratio of both asteroids. As noted earlier, Benner et al. (2007) found that all of the E-class objects in a survey of 160 NEAs had polarization ratios $\mu_c \geq 0.8$. Nysa's polarization ratio is lower than the NEA E-class sample and Hungaria's is at the lower end. Nevertheless, both values of μ_c are significantly higher than any other main-belt asteroid, suggesting a common cause. If we assume that the

compositional-cause hypothesis of Benner et al. is correct, we speculate that the lower polarization ratios of these MBAs compared with the NEA counterparts may be due to a greater amount of impact-related surface gardening and regolith accumulation because of their (likely) older surface age, greater surface gravity, or both.

A second feature of note is that Nysa and Hungaria have OC radar albedos $\hat{\sigma}_{OC} = 0.19$ - 0.22 . This is $\sim 50\%$ higher than the mean for MBAs found by Magri et al. (2007a) and is significant because a large fraction of the scattered radar power (the SC echo) is not included in the estimated radar albedo (*i.e.* if the surfaces had low polarization ratios, the radar albedos would be even higher). Since radar albedo is correlated with a surface bulk density, the uppermost meter or so of Nysa and Hungaria must have a bulk density higher than the typical MBA. Possible causes include low bulk porosity (coherent rock, greater population of rocks in the regolith, etc.), high metal content, or both (Magri et al. 2001; Shepard et al. 2007).

Future Opportunities

The next opportunities to observe main-belt E-class asteroids at Arecibo are in August 2009 when Hungaria will have SNRs $\sim 60\%$ greater than those shown here, Jan 2010 when 64 Angelina should have SNRs greater than ~ 15 /day, and February 2011 when Nysa will have SNRs similar to those shown here.

Acknowledgements

M.K.S. and K.M.K. gratefully acknowledge support from a NSF REU grant, AST-0605903. B.E.C. and M.E.O. were supported by NSF grant AST-0606704. C.M. was partially supported by NSF grant AST-0205975. The Arecibo Observatory is part of the National Astronomy and Ionosphere Center, which is operated by Cornell University under a cooperative agreement with the National Science Foundation. We thank the technical staff at the observatory for help with observations. Some of this work was performed at the Jet Propulsion Laboratory, California Institute of Technology, under contract with the National Aeronautics and Space Administration. This material is based in part upon work supported by the National Aeronautics and Space Administration (NASA) under the Science Mission Directorate Research and Analysis Programs.

References

- Bell, J.F., Davis, D.R., Hartmann, W.K., Gaffey, M.J. 1989. Asteroids: The big picture. In: Binzel, R.P, Gehrels, T., Matthews, M.S. (Eds.) Asteroids II, Univ. of Arizona, Tucson. pp. 921-948.
- Benner, L.A.M., Ostro, S.J., Magri, C., Nolan, M.C., Howell, E.S., Giorgini, J.D., Margot, J.L., Busch, M.W., Shepard, M.K., Taylor, P.A., Jurgens, R.F. 2007. Near-Earth asteroid surfaces: Macroscopic-scale roughness depends upon compositional class. Submitted to Science.
- Bus, S.J., Binzel, R.P. 2002. Phase II of the Small Main-Belt Asteroid Spectroscopic Survey: A Feature-Based Taxonomy. *Icarus* 158, 146-177.
- Campbell, B.A., Campbell, D. B. 1992. Analysis of volcanic surface morphology on Venus from comparison of Arecibo, Magellan, and terrestrial airborne radar data. *J. Geophys. Res.* 97, 16293-16314.
- Campbell, B.A., Campbell, D. B. 2006. Regolith properties in the south polar region of the Moon from 70-cm radar polarimetry. *Icarus* 180, 1-7.
- Durech, J., Scheirich, P., Kaasalainen, M., Grav, T., Jedicke, R., Denneau, L. 2007. Physical models of asteroids from sparse photometric data. In: Valsecchi, G.B. and Vokrouhlicky, D. (Eds.) Near Earth Objects, our Celestial Neighbors: Opportunity and Risk, Proceedings of IAU Symposium 236. Cambridge University Press, pp. 191-200.
- Harmon, J.K., Nolan, M.C. 2007. Arecibo radar imaging of Mars during the 2005 opposition. Seventh International Conference on Mars, abs. #3136.
- Harris, A.W., Young, J.W. 1983. Asteroid rotation. IV. 1979 Observations. *Icarus* 54, 59-109.

Harris, A.W., Young, J.W., Bowell, E., Tholen, D.J. 1999. Asteroid lightcurve observations from 1981-1983. *Icarus* 142, 173-201.

Kaasalainen, M., Torppa, J., Piironen, J. 2002. Binary structures among large asteroids. *Astron. & Astrophys.* 383, L19-L22.

Kelley, M.S., Gaffey, M.J. 2002. High-albedo asteroid 434 Hungaria: Spectrum, composition, and genetic connections. *Meteor. Planet. Sci.* 37, 1815-1827.

Magri, C., Consolmagno, G.J., Ostro, S.J., Benner, L.A.M., Beeney, B.R. 2001. Radar constraints on asteroid regolith properties using 433 Eros as ground truth. *Meteor. Planet. Sci.* 36, 1697-1709.

Magri, C., Nolan, M.C., Ostro, S.J., Giorgini, J.D. 2007a. A radar survey of main-belt asteroids: Arecibo observations of 55 object during 1999-2003. *Icarus* 186, 126-151.

Magri, C., Ostro, S.J., Dcheeres, D.J., Nolan, M.C., Giorgini, J.D., Benner, L.A.M., Margot, J.L., 2007b. Radar observations and a physical model of Asteroid 1580 Betulia. *Icarus* 186, 152-177.

Mitchell, D.L., Ostro, S.J., Hudson, R.S., Rosema, K.D., Campbell, D.B., Velez, R., Chandler, J.F., Shapiro, I.I., Giorgini, J.D., Yeomans, D.K., 1996. Radar observations of asteroids 1 Ceres, 2 Pallas, and 4 Vesta. *Icarus* 124, 113-133.

Morrison, D. 1977. Asteroid sizes and albedos. *Icarus* 31, 185-220.

Ostro, S.J., Hudson, R.S., Benner, L.A.M., Giorgini, J.D., Magri, C., Margot, J.L., Nolan, M.C., Asteroid radar astronomy, 2002. In: Bottke W. F. Jr., Cellino, A., Paolicchi, P., and Binzel, R. P. (Eds.), *Asteroids III*, Univ. of Arizona, Tucson, pp. 151-169.

Shepard, M.K., and 20 colleagues 2007. A radar survey of X- and M-class asteroids. Submitted to *Icarus*.

- Taylor, R.C., Tedesco, E.F. 1983. Pole orientation of Asteroid 44 Nysa via photometric astrometry including a discussion of the method's applications and limitations. *Icarus* 54, 13-22.
- Tedesco, E.F., Noah, P.V., Noah, M. 2002. The supplemental IRAS minor planet survey. *Astron. J.* 123, 1056-1085.
- Tholen, D.J. 1984. Asteroid taxonomy from cluster analysis of photometry. PhD thesis, Univ. of Arizona, Tucson. 150 pp.
- Tholen, D.J. and Barucci, M.A. 1989. Asteroid taxonomy. In: Binzel, R.P., Gehrels, T. and Matthews, M.S. (Eds.), *Asteroids II*, Univ. of Arizona, Tucson, pp. 298-315.
- Zellner, B., Leake, M., Morrison, D., Williams, J.G. 1977. The E-asteroids and the origin of the enstatite achondrites. *Geochim. Cosmochim. Acta* 41, 1759-1767.

Table 1 Asteroid Orbital and Physical Properties

Property	44 Nysa	434 Hungaria
a (AU)	2.42	1.94
e	0.148	0.074
i ($^\circ$)	3.7	22.5
H (mag)	7.03 ^a	11.21 ^b – 11.46 ^c
p_v	0.55 ^a	0.43 ^d
D (km)	68 ^b , 70.6 ^a , 73 ^e	8 ^b , 11 ^d
Class	E ^f , Xc ^g	E ^f , Xe ^g
P (h)	6.421417 ^{h,i}	26.51 ^{b,c} , 26.488 ^j
Δm	0.42-0.52 ^b	0.57 ^c -0.7 ^b
Pole ($\lambda^\circ, \beta^\circ$)	98, +58 ⁱ	119, +67 ^j

a is the orbital semi-major axis, e is the eccentricity, i is the inclination, H is the absolute magnitude, p_v is the visual albedo, D is the diameter, Class is the asteroid classification, P is the rotational period, Δm is the lightcurve amplitude, and Pole is the ecliptic coordinates of the rotation pole.

^aTedesco et al. 2002

^bHarris and Young (1983)

^cHarris et al. (1999)

^dMorrison (1977)

^eKelley and Gaffey (2002)

^fTholen (1985)

^gBus and Binzel (2002)

^hTaylor and Tedesco (1983)

ⁱKaasalainen et al. (2002)

^jDurech (personal comm.)

Table 2 Observation Circumstances

Target	Date (UTC)	RA (°)	DEC (°)	λ (°)	β (°)	# Runs	Δt (UTC)	Dist (AU)
44 Nysa	2006 Dec 22	100	19	99	-4	2	05:45-06:19	1.103
	2006 Dec 23	100	19	99	-4	2	04:14-05:30	1.101
	2006 Dec 24	99	19	99	-4	3	04:43-05:25	1.099
434 Hungaria	2006 May 14	244	19	237	40	5	04:17-06:27	0.979
	2007 May 16	243	20	236	40	4	04:06-05:44	0.979
	2008 May 18	243	20	236	41	4	03:57-05:08	0.979
	2009 May 20	242	21	235	41	5	03:47-05:57	0.979

RA is the right ascension, DEC is the declination, λ is the ecliptic longitude, and β is the ecliptic latitude at the time of acquisition; #runs is the number of transmit-receive cycles acquired on each date/time; Δt is the start-stop times of the receiving window; and Dist is the distance of the target from Earth.

Table 3 44 Nysa Radar Properties of Individual Runs

Date and time	UTC	OC			
		SNR	B_{EQ} (Hz)	σ_{oc} (km ²)	μ_c
2006 Dec 22	5:45	22	225±20	850±220	0.59±0.04
2006 Dec 22	6:19	17	280±20	950±240	0.51±0.05
2006 Dec 23	4:14	22	260±20	980±250	0.45±0.04
2006 Dec 23	5:30	20	315±20	980±250	0.54±0.05
2006 Dec 24	4:43	17	300±20	900±230	0.43±0.05
2006 Dec 24	5:25	25	245±20	1080±260	0.45±0.04
2006 Dec 24	6:02	20	250±20	900±230	0.53±0.04
Sum of all runs		52	400±50	950±240	0.50±0.02

For individual runs, we list the equivalent bandwidth, B_{EQ} , a conservative lower bound on bandwidth to give a sense of the variation in bandwidth (Magri et al. 2007a). The bandwidth listed for the sum of all runs is $B_{2\sigma}$, the point at which echo power drops to two standard-deviations of the noise level, and its uncertainties are based on the one-sigma and three-sigma crossing points. Uncertainties in cross-section are estimated to be 25% based on pointing and calibration uncertainties while those in polarization ratio are based on noise statistics.

Table 4 434 Hungaria Daily Radar Properties

Date	Runs	OC SNR	B_{EQ} (Hz)	σ_{oc} (km ²)	μ_c
2006 May 14	5	7	7±2	17±5	1.0±0.2
2006 May 16	4	8	9±2	25±7	0.6±0.1
2006 May 18	4	6	8±2	21±6	0.8±0.1
2006 May 20	5	8	9±2	22±6	0.8±0.2
Sum of all runs		15	12+3/-1	21±6	0.8±0.1

See note to Table 3.

44 Nysa

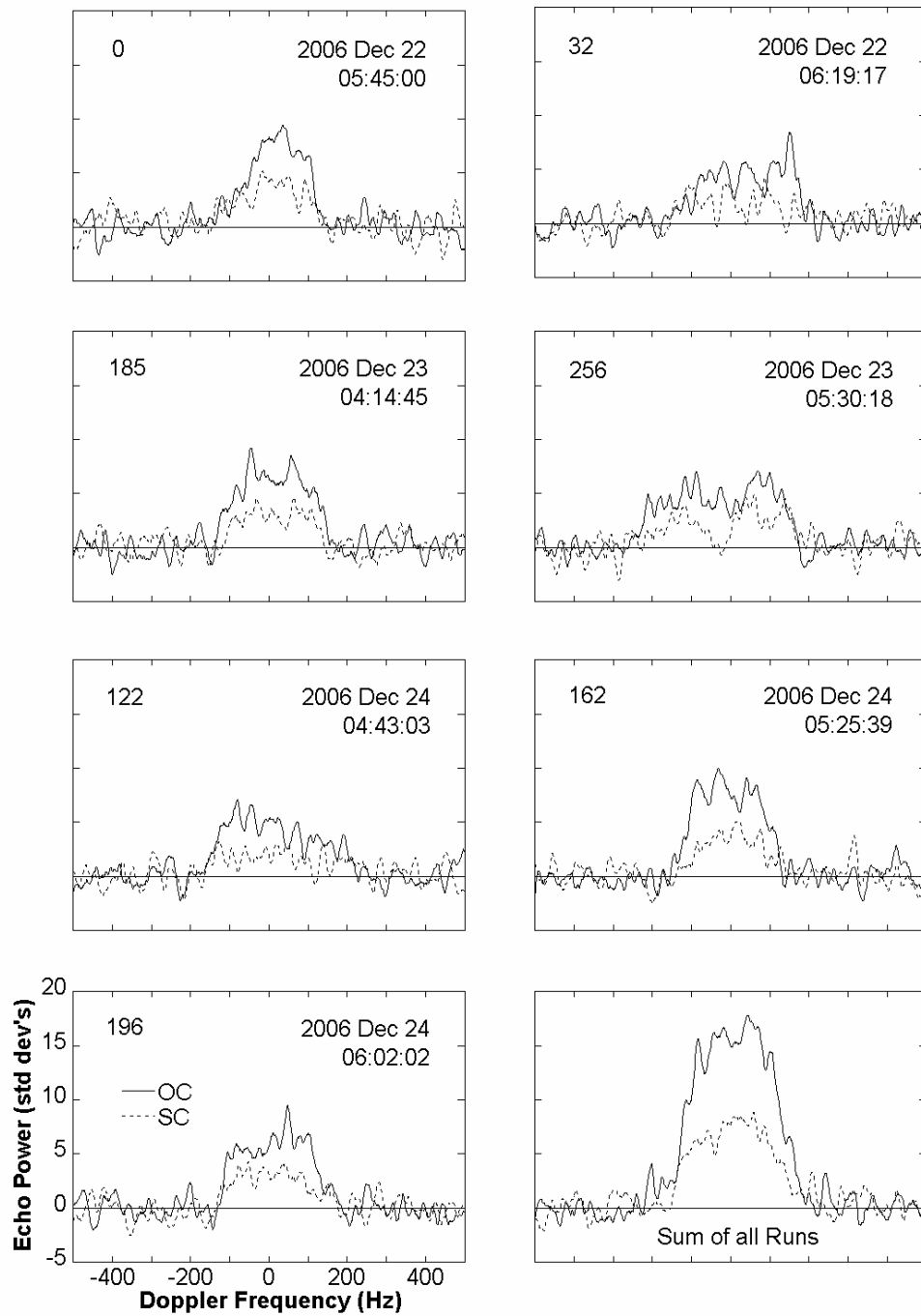


Figure 1. Radar observations of 44 Nysa. Date and time of observation mid-point are in upper right, rotation phase is in the upper left in degrees (starting with 0° for first run).

434 Hungaria

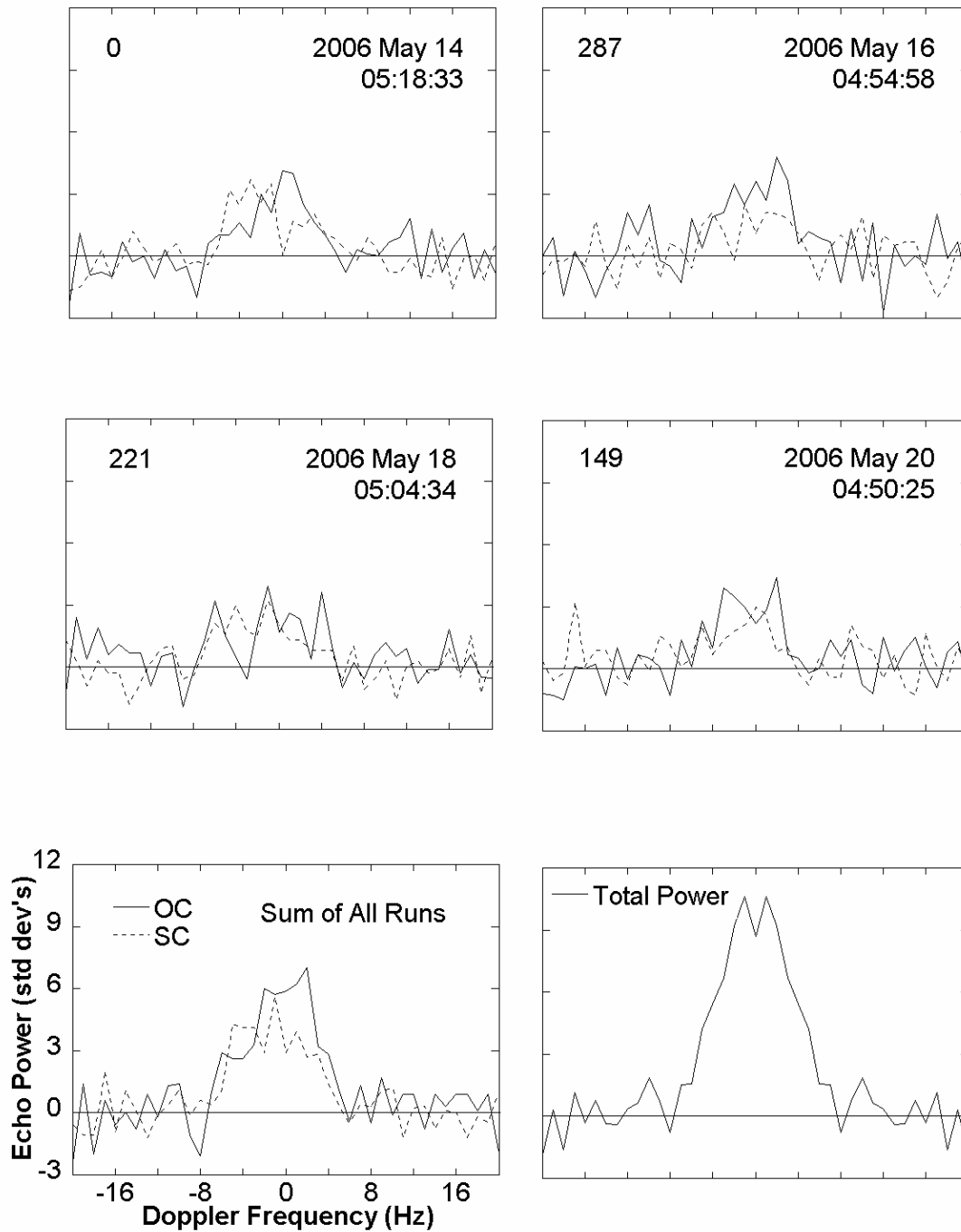


Figure 2. Daily radar observations of Hungaria (weighted sum of all runs on each date). Labels are the same as in Figure 1. The bottom two plots show the weighted sum of all runs (left) and the folded total-power spectrum sum of all runs (right).